

Comprehensive Understanding of Flicker Noise in Advanced FinFET Technology: from Noise Sources Separation to Physical-based Modeling

Junjie Wu^{1, #}, Pengpeng Ren^{1, #, *}, Chenyang Zhang¹, Yu Xiao¹, Yongkang Xue¹, Yu Li², Xiaolin Wang¹, Lining Zhang^{2, 5}, Junhua Liu^{3, 5}, Jianfu Zhang⁴, Runsheng Wang^{3, 5†}, Zhigang Ji^{1, 5*}, Ru Huang³

¹Department of Micro/Nano Electronics, SJTU, China (*pengpengren@sjtu.edu.cn; zhigangji@sjtu.edu.cn).

²ECE, PKU, Shenzhen, China. ³School of Integrated Circuits, PKU, China ([†]r.wang@pku.edu.cn).

⁴School of Engineering, LJMU, UK. ⁵Institute of EDA, PKU, Wuxi, China. [#]Equal contribution

Abstract—In this paper, a new physical-based model for flicker noise in advanced FinFET technology is proposed based on separation of intertwined noise sources. The proposed separation method can well clarify the sources of flicker noise, enabling the modeling of different components independently. The accuracy of this model is validated by the full-scale bias and device size dependencies of flicker noise, as well as its variations. It is observed that ignoring noise sources other than oxide traps can result in an underestimation of approximately 60% under operating condition. By introducing the equivalent circuit for simulation, the new model is readily to be used with commercial simulators for circuit-level analysis.

I. Introduction

Flicker noise has become a critical concern due to the increasing demand for analog/mixed signal circuits in advanced CMOS technologies [1]. However, the conventional corner model (Fig.2) tends to overestimate the impact of flicker noise due to severe device-to-device variations, rendering it intolerable. Moreover, the observed bias dependencies of single devices contradict the conventional understanding based on carrier number fluctuation (CNF) model [2] [3] (Fig.3). Even if the average experimental results of multiple devices are used, the number of defects extracted based on the CNF model is not physically meaningful (Fig.4). While the opinion prevailing in recent years attributes the origin of flicker noise to the superposition of random telegraph noise (RTN) from multiple traps [4], the limited number of traps on nanoscale devices fails to explain the nearly perfect 1/f slope observed in experimental results (Fig.5 & Fig.8a), indicating the existence of other noise sources. As a result, a correct understanding of the origin of flicker noise in nano-scaled devices is lacking, hindering the establishment of accurate statistical modelling.

To address this issue, we demonstrate the noise sources in industrial-grade 7nm FinFETs, revealing that the oxide traps, channel scattering, and access resistance are all contributors to the noise. By employing our proposed experimental separation method, we can understand the mechanism behind each noise source. Based on this understanding, we present a physics-based compact model that can be readily used for circuit-level simulations. **Importantly, we find that the prevailing understanding of multi-trap superposition is only valid when the operating voltage is close to the threshold voltage. When the operating voltage increases to the nominal VDD (~0.7V), ignoring the contribution of other noise sources can lead to an underestimation of approximately 60% (Fig.6).**

II. Statistical flicker noise model

A. Method for Noise Source Separation

In nano-scaled devices, flicker noise can originate from more than one sources: (de-)trapping in the dielectric layer for the oxide trap (OT)-induced noise; scattering of carriers during transport for channel scattering (CS)-induced noise; non-negligible source/drain access resistance (AR)-induced noise. For accurate modelling, the contribution of each noise source needs to be separated. The procedure is proposed in Fig.7. First, RTN causes the humps in the noise spectrum, leading to the deviation from the straight line (Fig.8a-c). The oxide trap-induced noise can be separated from the total by fitting the noise spectrum with Eq. 1. After removing oxide trap-induced noise, the current dependence of the normalized noise spectrum deviates from the conventional mobility fluctuation model (Fig.9) [5]. This can be ascribed to the non-negligible access resistance which not only contributes flicker noise but also leads to non-constant intrinsic drain bias under different I_D [6]. By fitting with Eq.13, the contribution of channel scattering- and access resistance-induced noise sources can be separated.

B. Channel Scattering (CS)-induced noise

Scattering between electrons and phonons and/or surface roughness causes mobility fluctuation, constituting the channel scattering-induced noise, which also exhibits strong device-to-device variations (Fig.10). CS-induced noise can be modeled with Hooge's empirical formula [5] using Eq.8 with Hooge parameter, α_H , which indicates the noise level related to the carrier mobility. By assessing each curve in Fig.10, α_H in each device can be obtained. The statistical information for α_H is analyzed (Fig. 11a-b). Wherein, μ_{α_H} shows very weak dependence on channel width while σ_{α_H} shows a clear decrease. This is because the devices with wider channels have stronger averaging effect. For the length dependence, μ_{α_H} decreases with a shorter channel because the quasi-ballistic transport becomes more remarkable (Fig.11c) [7]. This is further supported by the decreasing mobility with smaller α_H for shorter channels (Fig.12) [8]. σ_{α_H} exhibits a non-monotonic trend because a longer channel increases the variation due to enhanced scattering but reduces the variation due to averaging effect (Fig.11d). Moreover, the standard deviation of mobility and α_H have similar trend (Fig.13) [9], verifying the correlation between noise and carrier transport.

C. Access resistance (AR)-induced noise

Access resistance noise comes from the fluctuation of its current conduction. Similar to CS-induced noise, the AR-induced noise also shows strong variations because of the nano-scaled geometry (Fig.10). Such noise can be modeled with Eq.12 [6]. Wherein, the model parameter K_r shows strong dependence on W_{eff} but remains constant for different L_{eff} in terms of both the mean value and the deviation (Fig.16).

The fluctuation of series resistance can also affect channel current which in turn affects the CS-induced noise. This can be accounts through correction with Eq.13. R_{access} is required which is extracted as shown in Fig.9 for each device. R_{access} is found to follow the normal distribution with very weak channel length dependence (Fig.14). However, due to the averaging effect, R_{access} exhibits a strong dependence on the channel width. Both $\mu_{R_{access}}$ and $\sigma_{R_{access}}$ reduce with larger effective channel width (Fig.15a&b).

D. Oxide trap (OT)-induced noise

Oxide trap-induced noise represents itself as the random telegraph noise (RTN) in the time domain (Fig.17a). The widely-used elastic tunnelling is not valid to model RTN in advanced technology [12]. Instead, inelastic tunnelling based on multi-phonon-assisted non-radiative transition theory should be used [13]. By simplifying RTN as the two-state transition the key physical parameters of each trap including the energy level, E_t , the spatial location, X_t and the relaxation energy, S , can be obtained from the emission and capture time constants under different gate biases (Fig.17b). The extracted energy/spatial spectrum suggesting that these traps can exist in both IL and HK layers (Fig.17c).

We recently identified two types of pre-existing traps [14]. By comparing the trap properties extracted from DMP technique and the atomic simulation using density functional theory, it is found that Type-A traps are the oxygen vacancies located in the IL layer, and Type-B traps are mainly the hydroxyl E' in the HK layer [13,15]. Interestingly, when we compared the properties of the traps extracted from RTN technique, excellent agreement can be achieved for both Et and S if the comparison is made at IL and HK layers respectively (Fig.19). The good agreement from three independent studies strongly supports those traps account for the trapping-induced noise.

With highly-scaled geometry, strong interaction can occur if more than one trap exists in one device, leading to the coupling effect through the current percolation path or the Coulomb repulsion [16]. The coupling strengths can potentially affect the oxide trap-induced noise. One typical data with two-traps induced complex RTN presents evident impacts of the coupling effect. Both the fast and the slow trap can be successfully extracted from the measured current levels with Hidden Markov Model (HMM) algorithm [17] (Fig. 18a&b). The statistics of the coupling strength for Type A and Type B traps can be quite different: the stronger coupling observed in Type-A traps suggests that the distance between traps in IL layer could be closer than the traps in HK layer (Fig. 20a). The first principal calculation reveals that the formation energy in creating one Vo or hydroxyl E' near another neighbouring defect of the same type can be quite different. For Vo, the lowest formation energy position is found at site 3, with a distance of 7.8 Å, while for hydroxyl E', the lowest formation energy position is found at site 6, with a distance of 14.3 Å (Fig.20b-d). The coupling effect reduces the possibility of multiple trapping, which in turn reduces the contribution of oxide trap-induced noise.

The magnitude of the current change induced by the traps is another issue that needs to be addressed, especially its voltage dependence, which is critical for flicker noise prediction under any operating condition. Using our recently-proposed Dual-Point technique (DP) [18], the impact of each trap on the entire IV curve can be captured experimentally, which can be used to

extract the current change under any given Vg (Fig.22a). The extracted ΔV_{th} follows the exponential distribution (Fig.22b), the percentage in the voltage shift ($\Delta V/\Delta V_{th}$) shows very weak voltage dependence in both its mean value and standard deviation. For each trap, this statistical information ensures the modelling of ΔV at any Vg in Eq.7.

With comprehensive information on the traps in the dielectric, oxide trap-induced noise at the frequency domain under both DC and AC conditions can be calculated using multi-phonon-assisted non-radiative transition theory. What is worth noting is that the experimentally-observed frequency-dependent τ_c and frequency-independent τ_e can be well reproduced [19] (Fig.21a). By transforming into the frequency domain, PSD is found to show obvious reduction with higher clocker frequency. This frequency dependence along with the aforementioned coupling effect suggests that the oxide trap-induced noise could be over-estimated under circuit real operating conditions (Fig.21b).

III. Compact model & verification

The statistical flicker noise model can be constructed with Eq.2-15. Wherein the model parameters can be extracted from the experiment after noise source separation. The model is applicable for different channel length, width and also for statistical simulation under any operating condition (Fig.23-25). The accuracy of this model is verified by comparing between the experimental results and model prediction on devices under different biases (Fig.6&Fig.26). The noise distribution is affected by the uneven energy level distribution of oxide traps.

For noise analysis on circuit level, one voltage and one current source can be connected to each transistor (Fig.27a). Ring Oscillator with transistors of different sizes is used for demonstration (Fig.27b). Phase noise from oxide trap and channel scattering/access resistance are equally important, which increases with size shrinking (Fig.28a). MC simulation are also conducted to show the circuit variation (Fig.28b).

Finally, we benchmark our proposed model with the models reported recently in literature. Our model is the only type covering all three main noise sources with comprehensive capability (Table I).

VI. Conclusion

We have proposed a new predictive model for flicker noise in advanced FinFET technology. By separating multiple sources, a new noise model is established and equal importance of three noise sources are demonstrated. This model can well capture the frequency, bias and size dependencies of flicker noise, including its statistical characteristics. Equivalent circuit is also proposed for circuit-level analysis. This work is thus helpful to the variability-aware circuit design in advanced technology nodes.

ACKNOWLEDGMENT

The work is supported by National Key R&D Program of China (2019YFB2205005), NSFC (T2293700, T2293704, B18001)

REFERENCES

- [1] P. Kushwaha, *et al.*, *EDL* 2019. [2] A. McWhorter, *PR* 1955. [3] K. Hung, *et al.*, *TED* 1990. [4] M. Liu, *et al.*, *IEDM* 2021. [5] F. Hooge, *TED* 1994. [6] L. Vandamme, *et al.*, *TED* 2008. [7] S. Rakheja, *et al.*, *TED* 2015. [8] W. Wu, *et al.*, *TED* 2018. [9] R. Wang, *et al.*, *TED* 2011. [10] J. Campbell, *et al.*, *EDL* 2011. [11] R. Trevisoli, *et al.*, *TED* 2017. [12] R. Asanovski, *et al.*, *TED* 2021. [13] D. Waldhoer, *et al.*, *TED* 2021. [14] Y. Xue, *et al.*, *TED* 2023. [15] J. Lyons, *et al.*, *MEE* 2011. [16] S. Guo, *et al.*, *IRPS* 2018. [17] Z. Zhang, *et al.*, *IRPS* 2017. [18] X. Zhan, *et al.*, *EDL* 2019. [19] J. Zou, *et al.*, *VLSI* 2013. [20] H. Oka, *et al.*, *VLSI* 2020. [21] R. Kom Kammeugne, *et al.*, *IEDM* 2021. [22] R. Asanovski, *et al.*, *IEDM* 2022

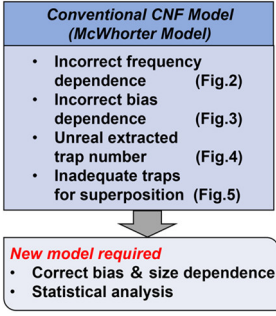


Fig.1 Conventional number fluctuation (CNF) model of flicker noise faces applicability challenges at nano-scaled region.

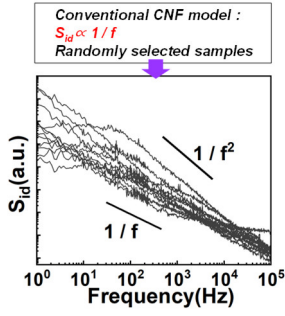


Fig.2 Measurement of flicker noise in nano-scaled FinFET. Some devices present ideal '1/f' noise, while the others deviate.

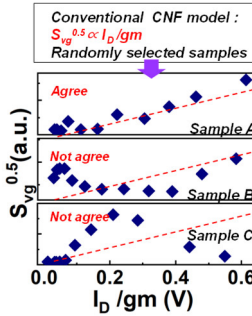


Fig.3 Measurement of flicker noise in nano-scaled FinFET deviates bias dependence of CNF model.

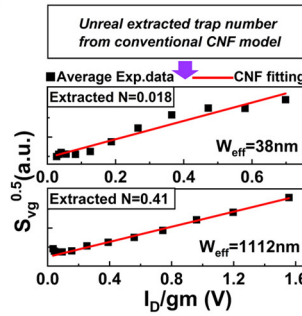


Fig.4 Extracted trap number from CNF model is too small to induce the measured flicker noise, which is not physical meaningful.

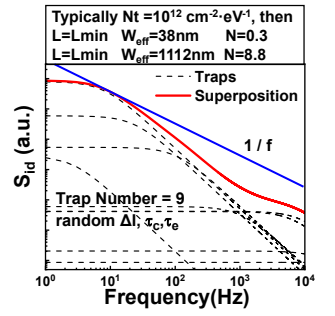


Fig.5 Assuming the trap density is $1E12 \text{ cm}^{-2} \text{ eV}^{-1}$ and all the traps can contribute to the flicker noise, the superposition of these traps can not restore the measured ideal '1/f' noise.

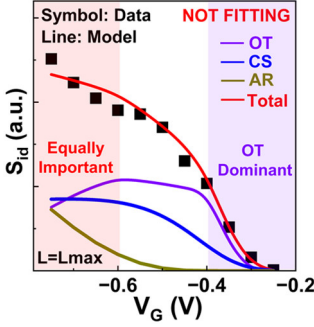


Fig.6 Comparison between the proposed model prediction and experiment data of S_{id} with different V_G on L_{max} device.

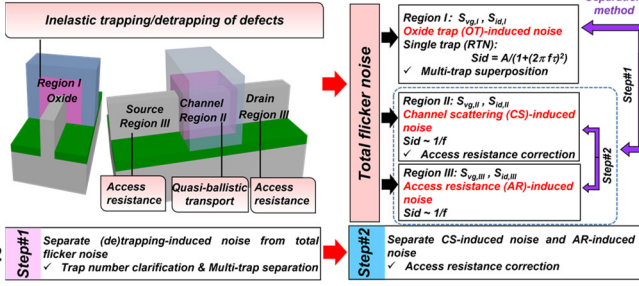


Fig.7 Several nonideal effects in nano-scaled FinFET, including inelastic (de)trapping of oxide defects, quasi-ballistic transport and parasitic access resistance, will contribute to the total flicker noise. Separation method of different noise components from different device regions is illustrated.

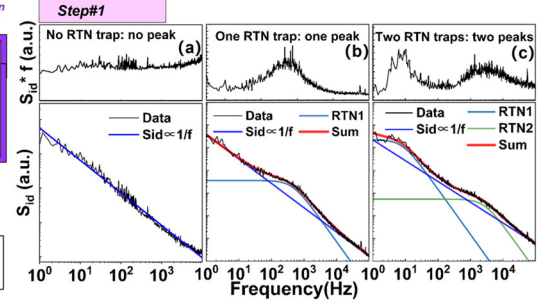


Fig.8 Illustration of separation of OR-induced noise from total flicker noise. The existence of RTN traps induces humps in the $S_{id} * f \sim f$ curves. By combining (multi-trap) RTN and '1/f' noise, the total flicker noise can be restored, from which the OR-induced noise can be separated.

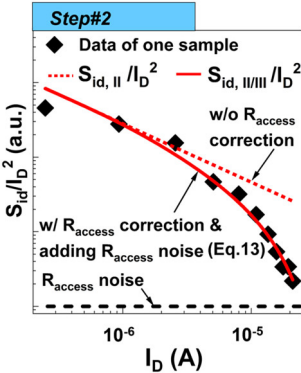


Fig.9 Illustration of the separation of CS-induced noise and AR-induced noise. With device downscaling, the impact of access resistance can not be neglected.

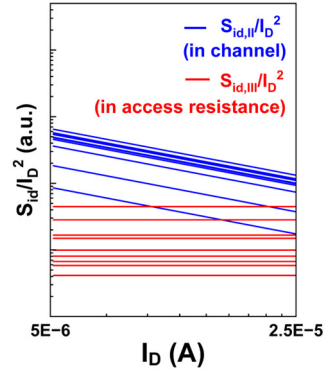


Fig.10 Separation results of CS-induced noise and AR-induced noise. Both components present severe variation, which require statistical analysis.

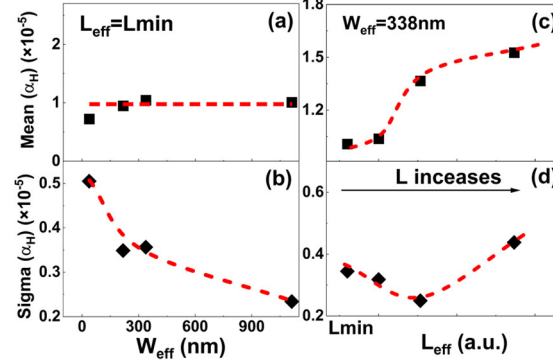


Fig.11 (a) Mean and (b) sigma values of extracted α_H with different channel width. (c) Mean and (d) sigma values of different channel length (b) extracted α_H with different channel length. It can be observed that the sigma of α_H present non-monotonic trend mobility. Both trend can be well captured by the proposed model.

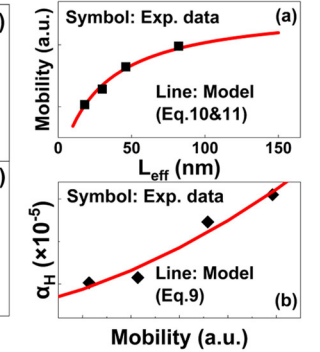


Fig.12 (a) Extracted mobility with different channel length. (b) Correlation between α_H and observed that the sigma of α_H present non-monotonic trend mobility. Both trend can be well captured by the proposed model.

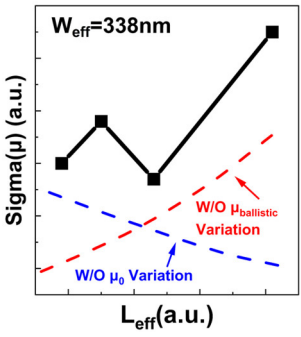


Fig.13. The trend of extracted sigma values of mobility with different channel length, which is a competing effect.

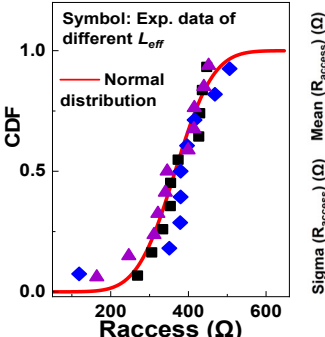


Fig.14 Distribution of extracted access resistance with different channel length, which shows weak dependence on L_{eff} and present normal distribution.

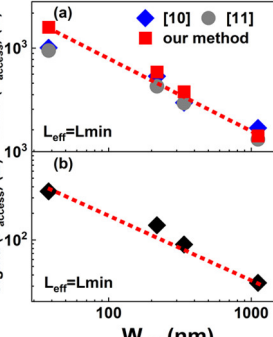


Fig.15 (a) Mean and (b) sigma values of extracted access resistance with different channel width, which is comparable with the results by other methods.

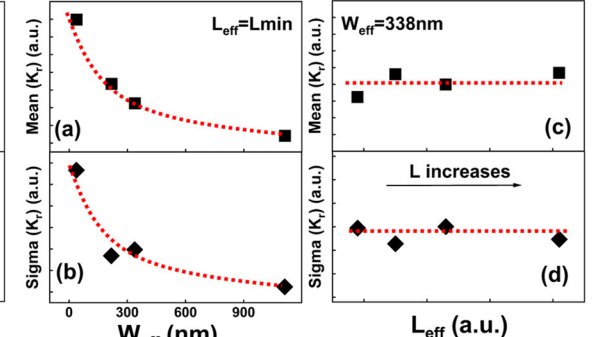


Fig.16 (a) Mean and (b) sigma values of extracted K_T in AR-induced noise with different channel width. (c) Mean and (d) sigma values of extracted K_T in AR-induced noise with different channel length.

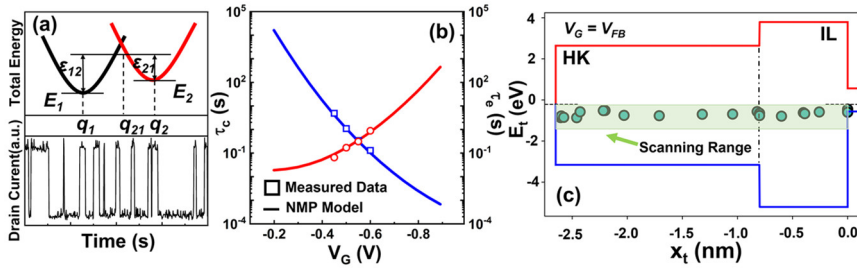


Fig.17 (a) Trap state transitions can be well described by the two state non-radiative multi-phonon (NMP) model. (b) Measured V_G dependence of the capture/emission time constants can be well described by two-state NMP model. (c) The band diagram of PMOS at $V_G = V_{FB}$ with oxide defects depicted according to their interface distance and energy level.

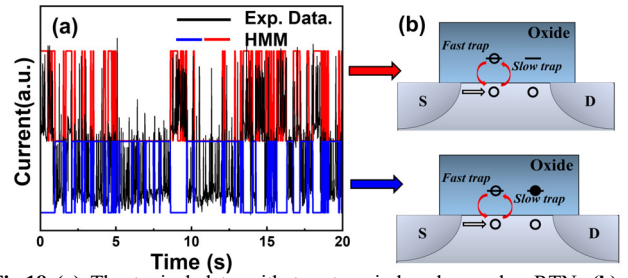


Fig.18 (a) The typical data with two-trap induced complex RTN. (b) Illustration of complex RTN caused by the two traps (a slow trap and a fast trap). RTN of individual traps can be specified.

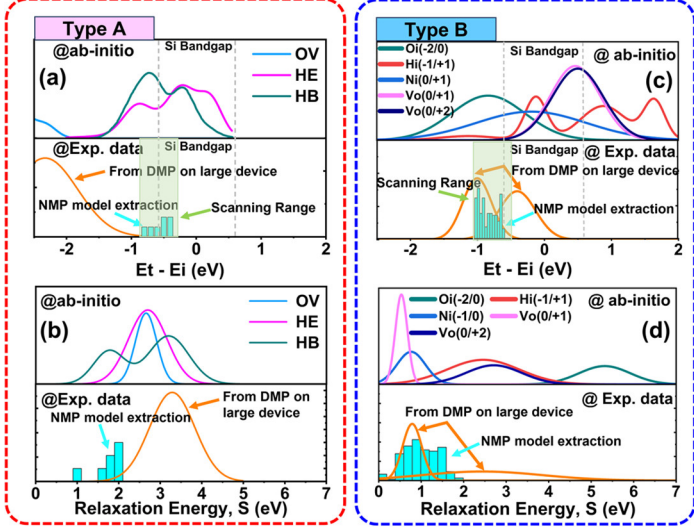


Fig.19 Comparison of the Ab-initio calculation, discharge-based multi-pulse (DMP) technique extraction [14] and NMP model extraction for (a) energy level and (b) relaxation energy of Type-A in the IL layer; (c) energy level and (d) relaxation energy of Type-B (B1 & B2) in the HK layer. Well agreement is achieved.

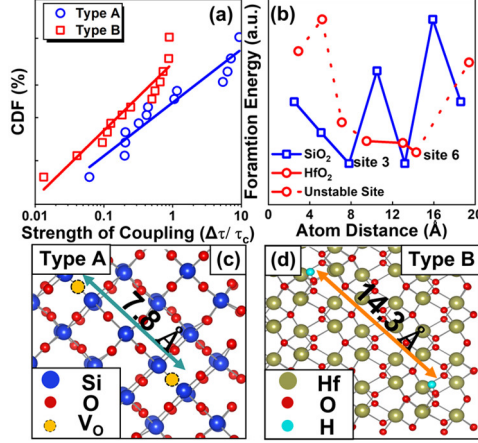


Fig.20 (a) The difference of coupling strength between Type-A and Type-B AC clock frequency [19]. (b) Simulated flicker noise under AC condition, which presents a decreasing trend with increasing AC clock frequency.

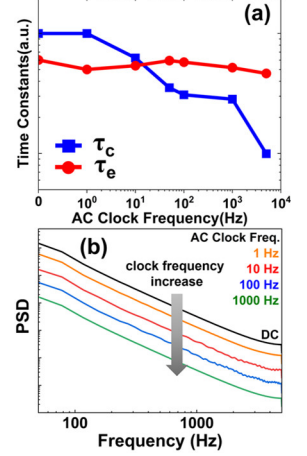


Fig.21 (a) The trend of time constants with AC clock frequency [19]. (b) Simulated flicker noise under AC condition, which presents a decreasing trend with increasing AC clock frequency.

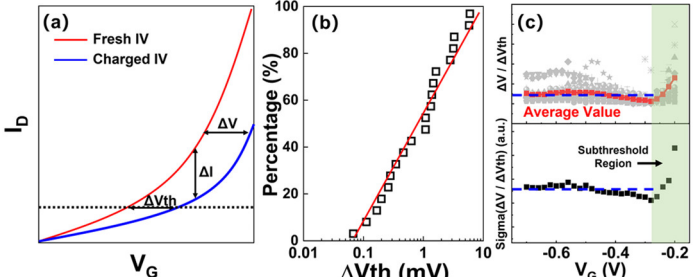


Fig.22 (a) Illustration of the device I_V curves before and after a single trap charging which can induce full I_V shift. (b) ΔV_{th} extracted by different devices manifest an exponential distribution. (c) Extracted V_G dependence of the mean and sigma values of normalized ΔV .

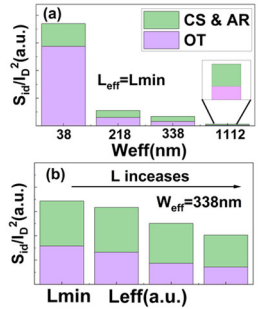


Fig.23 Contribution of OT, CS and AR induced noise in the total flicker noise under different (a) channel width and (b) channel length.

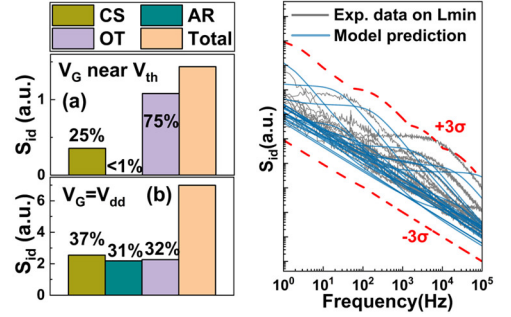


Fig.24 Contribution of OT, CS and AR induced noise in the total flicker noise under (a) V_{th} and (b) V_{dd} .

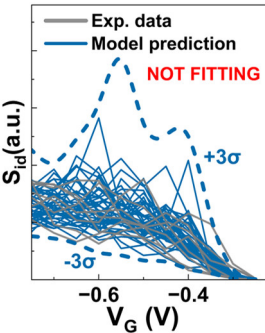


Fig.26 Comparison between the proposed model and exp. data with varying V_G bias. Statistical distribution is demonstrated on ring oscillator. NOT FITTING

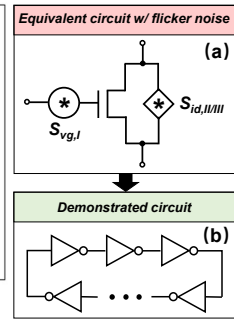


Fig.27 Illustration of the equivalent circuit of flicker noise (@1Mhz) under different channel length and (b) V_{DD} .

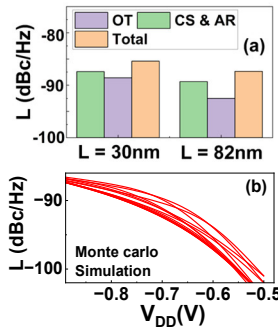


Fig.28 Simulated phase noise for different (a) channel length and (b) V_{DD} .

	2018 TED [8]	2020 VLSI [20]	2021 IEDM [4]	2021 IEDM [21]	2022 IEDM [22]	This work
Noise sources						
Oxide Traps	✓	✓	✓	✓	✓	✓
Channel Scattering	✓					✓
Access Resistance				✓		✓
Model feature						
Voltage dependence	✓	✓	✓	✓	✓	✓
Size dependence	✓			✓	✓	✓
Statistical analysis			✓			✓

Table I Benchmark of the proposed model with the reported models in literature.

Separation in frequency domain	
$S_{id} = \frac{K_c}{f} + \sum_{i=1}^N \frac{A_i}{1 + (2\pi f \tau_i)^2}$	$i = 0, 1, 2, \dots$ (1)
Region I (Gate oxide)	$N = N_t W L$ (2)
$\Delta V = m q / (W L C_{ox})$	$\tau_c = \frac{1}{pov_{th}} \exp(\epsilon_{12}/KT)$ (3)
$\tau_e = \tau_c \exp[-(E_f - E_c)/KT]$	$\epsilon_{12} = (S + E_{21})^2 / AS$ (4)
$S_{sig,i} = \sum_{i=1}^N (\tau_{ci} + \tau_{ei}) [(1/\tau_{ci} + 1/\tau_{ei})^2 + (2\pi f)^2]$	(5)
Region II (Channel)	$\frac{S_{id,II}}{I_D^2} = \frac{\alpha_H}{fN} = \frac{q\alpha_H \mu V_D}{f L^2 I_D}$ (6)
$\mu^{-1} = \mu_0^{-1} + \mu_{ballistic}^{-1}$	$\mu_{ballistic} = KL$ (7)
Region III (Access resistance)	$\frac{S_{id,III}}{I_D^2} = \frac{K_r}{f}$ (8)
(Access resistance correction)	
$S_{id,II/III} = S_{id,II} \left(\frac{R_{tot} - R_{access}}{R_{tot}} \right)^2 + S_{id,III} \frac{R_{access}^2}{2R_{tot}^2}$	(9)
$S_{id,II} = \theta_m^2 S_{sig,I}$	$S_{id} = S_{id,I} + S_{id,II/III}$ (10)
OT-induced noise	

Fig.25 Comparison between the proposed model and exp. data with varying frequency. $+3\sigma$ and -3σ